Received: 19 September 2022 | Accepted: 17 October 2022

DOI: 10.1002/pamm.202200016

Efficient micromagnetic finite element simulations using a perturbed Lagrange multiplier method

Maximilian Reichel[1,*], **Jörg Schröder**[1,**], and **Bai-Xiang Xu**[2,***]

[1] Institute of Mechanics, Faculty of Engineering, University of Duisburg-Essen, Universitätsstraße 15, 45141 Essen, Germany

[2] Division Mechanics of Functional Materials, Institute of Materials Science, Technical University Darmstadt, Otto-Berndt-Straße 3, 64287 Darmstadt, Germany

High performance magnets play an important role in critical issues of modern life such as renewable energy supply, independence of fossile resource and electro mobility. The performance optimization of the established magnetic material system relies mostly on the microstructure control and modification. Here, finite element based in-silico characterizations, as micromagnetic simulations can be used to predict the magnetization distribution on fine scales. The evolution of the magnetization vectors is described within the framework of the micromagnetic theory by the Landau-Lifshitz-Gilbert equation, which requires the numerically challenging preservation of the Euclidean norm of the magnetization vectors. Finite elements have proven to be particularly suitable for an accurate discretization of complex microstructures. However, when introducing the magnetization vectors in terms of a cartesian coordinate system, finite elements do not preserve their unit length a priori. Hence, additional numerical methods have to be considered to fulfill this requirement. This work introduces a perturbed Lagrangian multiplier to penalize all deviations of the magnetization vectors from the Euclidean norm in a suited manner. To reduce the resulting system of equations, an element level based condensation of the Lagrangian multiplier is presented.

1 Introduction

Magnets can be classified into magnetically soft and hard materials. Here, the terms “hard” and “soft” refer to the switching resistance of magnetic materials in the presence of externally applied magnetic fields. Soft magnetic materials are featured by slender hysteresis loops, in contrast to hard magnetic materials, that have particularly wide hysteresis loops [16]. These differently pronounced characteristics inherently lead to different fields of application of the materials. However, both hard and soft magnetic materials make a significant contribution to further increasing the efficiency of power generators (wind turbines), conversion equipment (transformers), sensors and means of transport (electromobility), as discussed in [1]. Significantly enhanced properties of these magnetic materials are a key to improving energy efficiency, contributing substantially to flexible and intelligent designs of industrial applications as well as reducing their environmental impact. Nevertheless, energy consumption always leaves an environmental footprint that, most importantly, must be minimized. Therefore, improving the energy chain (conversion-storage-transport and reconversion) is of crucial importance [2]. Promising potential for improvement is shown by both the synthesis of novel chemical compositions of materials and new processing techniques for microstructures. The enhancement of such processing routes may be of crucial importance to further enhance the performance of magnets. As already small defects, e.g. misoriented grains within the microstructure of a permanent magnet, may lead to decreasing values in coercivity [3], that differ from theoretically attainable values. The large discrepancy between the theoretically and practically obtained coercivity is well known as ’Brown’s paradox’ [4]. To meet and ultimately overcome this issue, a deep understanding of magnetic materials is necessary. Such a deep understanding aims to be achieved by interdisciplinary research teams starting with investigations from the atomistic scale (Å) up to the macroscopic scale (mm) [5]. On those different scales, various methods are used to investigate the magnetic phenomena. One of these scales to be analyzed is the micron scale. To understand the complex phenomena of magnetism on that scale, the micromagnetic theory has been established as a suited tool. It allows for the observation of magnetic domains and their very dynamic motions as well as for the analysis of the materials hysteresis properties. The physical phenomena associated with magnetization dynamics can be described precisely using the Landau-Lifshitz-Gilbert equation (LLG) [6, 7]. For instance, micromagnetism is applied to numerically investigate microstructures regarding their magnetic properties and the influences of varying geometries and chemical compositions as done by [8–10] among others. Since the considered materials are far below their Curie temperature the magnetization magnitude remains constant, i.e. $||\boldsymbol{M}|| = M_s$, where $\boldsymbol{M}$ is the magnetization vector and M_s the saturation magnetization. This requirement provides a numerically challenging constraint, that can be enforced by, among others, projection methods [11, 12], penalty methods [11, 13] or a priori length preserving strategies [14, 24]. Within this work the constraint is enforced by a perturbed Lagrange multiplier method as proposed by [22]. For the general treatment of the latter the readers are referred to [18] and [19]. The multiplier is an additional degree of freedom that penalizes any deviation of the magnetization vectors from

* Corresponding author: e-mail maximilian.reichel@uni-due.de, phone +49 201 183 6647, fax +49 201 183 2680

** e-mail j.schroeder@uni-due.de, phone +49 201 183 2682, fax +49 201 183 2680

*** e-mail xu@mfm.tu-darmstadt.de, phone +49 6151 16 21906, fax +49 6151 16 21906

the required length in a suited intensity, since the intensity is recalculated within each iteration step. However, the drawback is a larger system of equations resulting in higher computational effort during the solution procedure. To reduce this effort a condensation of the Lagrange multiplier within the local system of equations is performed, utilizing the Schur complement. To demonstrate the workability of the presented method, the magnetic properties of a nano structure consisting of permalloy are investigated. The nano structure is not only subjected to magnetic loading, but also to mechanical and magnetic loading.

This work is structured in the following manner: *Firstly,* all governing equations along with their corresponding boundary conditions are introduced to fully describe the micromagnetic-mechanically coupled boundary value problem. *Secondly,* the energy functional including all important contributing energies is presented. *Thirdly,* the finite element implementation of the beforehand introduced field equations is discussed. *Fourthly,* The workability of the proposed method is presented in terms of a suited numerical example, followed by a concluding section.

2 Field equations

The coupling between mechanical and magnetic properties is of significant importance for the simulation and design of ferromagnetic materials. The magnetic properties can be stimulated by mechanical influences. In this paper we assume small deformations and thus a linear elastic material behavior. Hence, the quasi-static states of the deformations within a body $\mathcal{B} \subset \mathbb{R}^3$ parametrized in $\boldsymbol{x}$ can be described via the balance of linear momentum

$$\operatorname{div} \boldsymbol{\sigma} + \boldsymbol{f} = \boldsymbol{0} \quad \text{in} \quad \mathcal{B}, \tag{1}$$

where $\boldsymbol{\sigma}$ denotes the Cauchy stress tensor and $\boldsymbol{f}$ the acting body force vector. The small deformation assumption leads to the following symmetric strain tensor

$$\boldsymbol{\varepsilon} = \frac{1}{2}\left[\nabla \boldsymbol{u} + (\nabla \boldsymbol{u})^{\mathrm{T}}\right], \tag{2}$$

that can be derived utilizing the definition of the spatial gradient $\nabla(\cdot) = \partial(\cdot)/\partial \boldsymbol{x}$. Suited boundary conditions on $\partial\mathcal{B} = \partial\mathcal{B}_u \cup \partial\mathcal{B}_\sigma$, with $\partial\mathcal{B}_u \cap \partial\mathcal{B}_\sigma = \emptyset$ can be prescribed either as Dirichlet- or Neumann-type boundary conditions as

$$\boldsymbol{u} = \boldsymbol{u}_0 \quad \text{on } \partial\mathcal{B}_u \qquad \text{and} \qquad \boldsymbol{\sigma} \cdot \boldsymbol{n} = \boldsymbol{t}_0 \quad \text{on } \partial\mathcal{B}_\sigma, \tag{3}$$

respectively. Here, $\boldsymbol{u}_0$ denotes the an arbitrarily prescribed displacement and $\boldsymbol{t}_0$ the acting traction vector. The evolution of the magnetic field considered here can be described by the magnetic gauss law

$$\operatorname{div} \boldsymbol{B} = 0 \quad \text{with} \quad \boldsymbol{B} = \boldsymbol{\mu} \cdot (\boldsymbol{H} + \boldsymbol{M}), \tag{4}$$

where $\boldsymbol{B}$ denotes the magnetic induction, depending on the magnetic field $\boldsymbol{H}$ and the magnetization $\boldsymbol{M}$. The material dependent magnetic permeability tensor is represented by $\boldsymbol{\mu}$. Let φ be a scalar magnetic potential, then the magnetic field can be gained from the relation

$$\boldsymbol{H} := -\nabla \varphi. \tag{5}$$

To fully describe the boundary value problem the boundary conditions on $\partial\mathcal{B} = \partial\mathcal{B}_\varphi \cup \partial\mathcal{B}_B$, with $\partial\mathcal{B}_\varphi \cap \partial\mathcal{B}_B = \emptyset$ corresponding to the scalar potential can be defined as

$$\varphi = \varphi_0 \quad \text{on } \partial\mathcal{B}_\varphi \qquad \text{and} \qquad \boldsymbol{B} \cdot \boldsymbol{n} = \zeta_0 \quad \text{on } \partial\mathcal{B}_B. \tag{6}$$

Since the induction is a function of the magnetic field as well as the magnetization, which is variable in space and time, an evolution equation describing the the magnetization dynamics is required. This dynamic behavior is suitably represented in the micromagnetic theory by the Gilbert equation, that can be expressed as

$$\dot{\boldsymbol{m}} = -\gamma_0 \mu_0 \, \boldsymbol{m} \times \boldsymbol{H}^{\mathrm{eff}} + \alpha \, \boldsymbol{m} \times \dot{\boldsymbol{m}}. \tag{7}$$

The physical constants γ_0 and μ_0 are the gyromagnetic ratio as well as the permeability of a vacuum, while α defines the material dependent Gilbert damping parameter, $\dot{\boldsymbol{m}}$ describes the rate of the magnetization vectors and $\boldsymbol{H}^{\mathrm{eff}}$ the so-called effective field. Here it must be noticed that the magnetization within the magnetic solid $\mathcal{B}$ is defined by the relation $\boldsymbol{M} := M_s \, \boldsymbol{m}$, where $\boldsymbol{m}$ represents the magnetic unit director. However, outside of $\mathcal{B}$ it holds $\boldsymbol{M} := \boldsymbol{0}$. In general, micromagnetism assumes isothermal conditions far below the Curie temperature of the considered material, so that the magnetization requires the constraint

$$||\boldsymbol{M}|| = M_s \quad \text{and} \quad ||\boldsymbol{m}|| = 1. \tag{8}$$

In the context of the present work, $||\boldsymbol{m}|| = \sqrt{\boldsymbol{m} \cdot \boldsymbol{m}}$ denotes the Euclidean norm.

3 Energy functional

To precisely describe the magnetization behavior of magnetic solids within the micromagnetic theory, the knowledge of the competing internal as well as external energies is required. Here, these energies are assembled within the energy functional as

$$\mathcal{H}\left(\boldsymbol{\varepsilon}, \boldsymbol{H}, \boldsymbol{m}, \nabla \boldsymbol{m}\right) = \mathcal{H}^{\mathrm{ela}}(\boldsymbol{\varepsilon}, \boldsymbol{m}) + \mathcal{H}^{\mathrm{mag}}(\boldsymbol{H}, \boldsymbol{m}) + \mathcal{H}^{\mathrm{exc}}(\nabla \boldsymbol{m}) + \mathcal{H}^{\mathrm{ani}}(\boldsymbol{m}). \tag{9}$$

The elastic term $\mathcal{H}^{\mathrm{ela}}$ includes mechanical effects on the magnetic solid, while the magnetostatic part $\mathcal{H}^{\mathrm{mag}}$ is responsible for the formation of magnetic domains and the magnetic exchange term $\mathcal{H}^{\mathrm{exc}}$ causes the parallel alignment of the magnetic moments. The influence of the crystalline lattice on the magnetic properties is addressed by the crystalline anisotropy $\mathcal{H}^{\mathrm{ani}}$. This can be formally defined as follows

$$\begin{aligned} &\mathcal{H}^{\mathrm{ela}}(\boldsymbol{\varepsilon}, \boldsymbol{m}) = \frac{1}{2}\boldsymbol{\varepsilon}^{\mathrm{e}} : \mathbb{C} : \boldsymbol{\varepsilon}^{\mathrm{e}}, \quad \mathcal{H}^{\mathrm{mag}}(\boldsymbol{H}, \boldsymbol{m}) = -\frac{1}{2}\mu_0\, \boldsymbol{H}\cdot\boldsymbol{H} - \mu_0 M_s \boldsymbol{H}\cdot\boldsymbol{m} \\ &\mathcal{H}^{\mathrm{exc}}(\nabla \boldsymbol{m}) = 2A_{\mathrm{exc}} \nabla \boldsymbol{m} : \nabla \boldsymbol{m} \quad \text{and} \quad \mathcal{H}^{\mathrm{ani}}(\boldsymbol{m}) = K_{\mathrm{ani}}\left(\boldsymbol{m}\cdot\boldsymbol{a}\right), \end{aligned} \tag{10}$$

where $\mathbb{C}$ denotes the mechanical stiffness tensor, $\boldsymbol{\varepsilon}^{\mathrm{e}} = \boldsymbol{\varepsilon} - \boldsymbol{\varepsilon}^{0}$ the elastic strain tensor, $\boldsymbol{\varepsilon}^{0} = \lambda_{100}\frac{3}{2}\left(\boldsymbol{m}\otimes\boldsymbol{m} - \frac{1}{3}\boldsymbol{I}\right)$ the magnetization induced strain tensor, λ_{100} the magnetostrictive coefficient, A_{exc} the exchange coefficient, K_{ani} the anisotropy parameter and $\boldsymbol{a} = \left[\sin\theta_1\cos\theta_2, \sin\theta_1\sin\theta_2, \cos\theta_1\right]^T$ a structural vector indicating the preferred direction of the material. The magnetization vectors will be subject to a torque developed by the so-called effective field [25]. This effective field is derived via the relation

$$\boldsymbol{H}^{\mathrm{eff}} = \frac{-1}{\mu_0 M_s}\left[\boldsymbol{\pi} - \operatorname{div}\boldsymbol{\Pi}\right], \quad \text{with} \quad \boldsymbol{\pi} = \frac{\partial\,\mathcal{H}}{\partial\,\boldsymbol{m}} \quad \text{and} \quad \boldsymbol{\Pi} = \frac{\partial\,\mathcal{H}}{\partial\,\nabla\boldsymbol{m}}. \tag{11}$$

4 Finite element implementation

For the solution of micromagnetic-mechanically coupled boundary value problems, based on the finite element method (FEM), the equations introduced in Sect. 2 have to be transferred into their weak forms. The solution procedure invokes in most cases some Newton-like methods, that also requires the corresponding linear increments of the considered equations. Since these linear increments might result in complicated derivations the whole system of equations is derived and implemented into the framework of AceGen/AceFEM [20] which possesses a strong automatic differentiation engine. A general overview of the FEM is provided in [18].

4.1 Weak forms of field equations and enforcement of unit constraint with a Lagrange multiplier

The weak forms of the field equations outlined in Sect. 2 can be stated as

$$\begin{aligned} G_u &= -\int_{\mathcal{B}} \delta\boldsymbol{\varepsilon} : \boldsymbol{\sigma}\ \mathrm{dv} + \int_{\partial\mathcal{B}_\sigma} \delta\boldsymbol{u}\cdot\boldsymbol{t}_0\ \mathrm{da}, \quad G_\varphi = -\int_{\mathcal{B}} \delta\boldsymbol{H}\cdot\boldsymbol{B}\ \mathrm{dv} + \int_{\partial\mathcal{B}_B} \delta\varphi\,\zeta_0\ \mathrm{da}, \\ G_m &= -\int_{\mathcal{B}} \left\{\delta\boldsymbol{m}\cdot\left[\frac{M_s}{\gamma_0}(\alpha\,\dot{\boldsymbol{m}} + \boldsymbol{m}\times\boldsymbol{m}) + \mathbb{P}\cdot\partial_{\boldsymbol{m}}\mathcal{H}\right] + \nabla\delta\boldsymbol{m} : \boldsymbol{\Pi}\right\}\mathrm{dv} + \int_{\mathcal{B}} 2\ \delta\boldsymbol{m}\cdot\boldsymbol{m}\ \lambda\ \mathrm{dv}, \end{aligned} \tag{12}$$

where $\delta\boldsymbol{u}, \delta\boldsymbol{\varepsilon}, \delta\varphi, \delta\boldsymbol{H}, \delta\boldsymbol{m}$ and $\delta\nabla\boldsymbol{m}$ denote the variational counterparts of the primary variables and their spacial derivatives. The time derivative of the magnetization is indicated as $\dot{\boldsymbol{m}}$ and $\mathbb{P} = (\boldsymbol{I} - \boldsymbol{m}\otimes\boldsymbol{m})$ represents an abbreviation for compact notation. Since the considered unit constraint on the magnetization vectors is not fulfilled a priori, it is enforced via a Lagrange multiplier λ. Here, an additional degree of freedom is added to the system of equations, that penalizes all deviations of the magnetization vectors from the Euclidean norm with a suited intensity, since it is recalculated within each iteration step. One disadvantage of Lagrange multipliers is obviously that the system of equations grows by an additional degree of freedom, increasing the computational effort during the solution procedure. Another disadvantage is, the saddle point structure of the system matrix which can lead to problems during the solution procedure, especially with iterative solvers involved, compare [17] or [18]. To circumvent the latter problem, instead of a classical Lagrangian formulation as presented in [21], a perturbed formulation, proposed by [22], is applied. The weak form of the perturbed Lagrange functional yields

$$G_\lambda = \int_{\mathcal{B}} \delta\lambda\left(\left[||\boldsymbol{m}||^2 - 1\right] - \frac{\lambda}{k_L}\right)\ \mathrm{dv}, \tag{13}$$

where $\delta\lambda$ denotes the variational counterpart of the Lagrange multiplier. Due to the squared Lagrange multiplier and the scaling factor k_L non-zero entries are generated on the main diagonal, which leads to less numerical difficulties, compare also [17] or [18]. To shorten the notation $\underline{(\cdot)}$ denotes arrays and the abbreviation $\Xi^T := \{\boldsymbol{u}^T, \varphi, \boldsymbol{m}^T\}$ holds in the following. From

the above introduced weak forms G_Ξ, G_λ and their corresponding linear increments, the local residual $\underline{\mathbb{R}}^T = \left[\underline{\mathbb{R}}_\Xi^T,\ \underline{\mathbb{R}}_\lambda^T\right]^T$ as well as the corresponding system matrix $\underline{\mathbb{K}}$ of the current iteration, can be obtained and represented as the following system of equations:

$$\begin{bmatrix} \underline{\mathbb{R}}_\Xi \\ \underline{\mathbb{R}}_\lambda \end{bmatrix} = \begin{bmatrix} \underline{\mathbb{K}}_{\Xi\Xi} & \underline{\mathbb{K}}_{\Xi\lambda} \\ \underline{\mathbb{K}}_{\lambda\Xi} & \underline{\mathbb{K}}_{\lambda\lambda} \end{bmatrix} \begin{bmatrix} \Delta\underline{\boldsymbol{d}}_\Xi \\ \Delta\underline{d}_\lambda \end{bmatrix}, \tag{14}$$

where $\Delta\underline{\boldsymbol{d}}_\Xi$ and $\Delta\underline{d}_\lambda$ are the incremental degrees of freedom of the coupled system.

4.2 Interpolation space of the Lagrange multiplier

With the definition of a scalar-valued function $a \in \mathbb{R}$, the $L^2(\mathcal{B})$-space can be formally expressed as $L^2 := \{a : ||a||_{L^2} < \infty\}$, with $||a||_{L^2(\mathcal{B})} = \sqrt{\int_\mathcal{B} |a|^2 \,\mathrm{dv}}$ defining the corresponding $L^2(\mathcal{B})$-norm for scalar valued functions a on the domain $\mathcal{B} \in \mathbb{R}^3$. The approximation of the Lagrange multiplier in the function space

$$\Lambda_j^h = \left\{ \lambda \in L^2\left(\mathcal{B}\right)^3 : \lambda|_{\mathcal{B}_e} \in P_j^d\left(\mathcal{B}_e\right)^3 \ \forall\, \mathcal{B}_e \right\}, \tag{15}$$

utilizes discontinuous Lagrangian type finite element interpolation functions $P_j^d(\mathcal{B}_e)^3$, where j denotes the considered interpolation orders. Since $\lambda \in L^2\left(\mathcal{B}\right)^3$ no special continuity requirements are requested, which allows for a static condensation.

4.3 Condensation of the Lagrange multiplier

The Schur decomposition allows to reduce the dimension of the local system of equations by a static condensation of the degrees of freedom, also compare [20]. Within the context of this work, the degree of freedom to condense is the Lagrange multiplier. Hence, the system of equations in Eq. 14 is decomposed and reassembled leading to the reduced system of equations

$$\underline{\mathbb{R}}_\mathrm{c} = \underline{\mathbb{K}}_\mathrm{c}\ \Delta\underline{\boldsymbol{d}}_\mathrm{c}, \quad \text{with} \quad \underline{\mathbb{R}}_\mathrm{c} = \underline{\mathbb{R}}_\Xi - \underline{\mathbb{K}}_{\Xi\lambda} \underbrace{\underline{\mathbb{K}}_{\lambda\lambda}^{-1} \underline{\mathbb{R}}_\lambda}_{\underline{\mathbf{L}}_\lambda} \quad \text{and} \quad \underline{\mathbb{K}}_\mathrm{c} = \underline{\mathbb{K}}_{\Xi\Xi} - \underline{\mathbb{K}}_{\Xi\lambda} \underbrace{\underline{\mathbb{K}}_{\lambda\lambda}^{-1} \underline{\mathbb{K}}_{\lambda\Xi}}_{\underline{\mathbf{L}}_{\lambda\Xi}}. \tag{16}$$

The update of the local degrees of freedom associated to the Lagrange multiplier follows the rule

$$\underline{d}_\lambda = \underline{d}_\lambda^n + \underline{\mathbf{L}}_\lambda - \underline{\mathbf{L}}_{\lambda\Xi}\, \Delta\underline{\boldsymbol{d}}_\Xi^n. \tag{17}$$

The new system matrix was reduced by one degree of freedom and thus corresponds to the dimensions of a system matrix in which the unit constraint is observed by a penalty parameter.

5 Numerical examples

Magnetic nano structures that are able to develop a vortex are of particular interest as they can play an important role in the development of magnetic storage media [23]. These nano structures are mostly measured between some 10 nm up to a few μm thick [23]. To demonstrate the workability of the proposed method a nano structure of Permalloy ($Ni_{80}Fe_{20}$) and the corresponding dimensions of $250\,\mathrm{nm} \times 250\,\mathrm{nm} \times 20\,\mathrm{nm}$ is considered within this contribution. Magnetic fields form around a magnetic solid and can have a strong influence on its behavior. To numerically consider these fields, the considered magnet must be surrounded by a free space discretized by means of finite elements. The free space considered here is of dimensions $2000\,\mathrm{nm} \times 2000\,\mathrm{nm} \times 1000\,\mathrm{nm}$. The material parameters can be taken from Tab. 1. The Gilbert damping parameter of Permalloy is usually assumed to be of amplitude around $\alpha = 0.008$, but to faster adapt the quasi-static magnetization states, this parameter is considered to be slightly higher as $\alpha = 0.5$, what is a common assumption in micromagnetic simulations and does not influence the results significantly, compare [23, 26]. At the beginning, the nano structure is initiated with an energetically high random distribution of the magnetization vectors (Fig. 1a and c) that is subsequently relaxed to its energetically more favorable self-equilibrium state (Fig. 1b and d), without the influence of any external magnetic or mechanical influences. This self-equilibrium state corresponds to a so-called vortex state and serves as the initial configuration for subsequent

Table 1: Material parameters of permalloy ($Ni_{80}Fe_{20}$) are taken from [26] and [24] .

Parameter		Unit	$Ni_{80}Fe_{20}$	Parameter		Unit	$Ni_{80}Fe_{20}$
exchange const.	A_e	$/\frac{\mathrm{J}}{\mathrm{m}}$	$1.3 \cdot 10^{-11}$	sat. magnetization	M_s	$/\frac{\mathrm{A}}{\mathrm{m}}$	$8 \cdot 10^{5}$
vac. permeability	μ_0	$/\frac{\mathrm{H}}{\mathrm{m}}$	$4\pi \cdot 10^{-7}$	anisotropy const.	K_{ani}	$/\frac{\mathrm{J}}{\mathrm{m}^3}$	0
elastic const.	$\mathbb{C}_{11}$	$/\frac{\mathrm{N}}{\mathrm{m}^2}$	$1.27 \cdot 10^{11}$	elastic const.	$\mathbb{C}_{12}$	$/\frac{\mathrm{N}}{\mathrm{m}^2}$	$0.75 \cdot 10^{11}$
elastic const.	$\mathbb{C}_{44}$	$/\frac{\mathrm{N}}{\mathrm{m}^2}$	$0.52 \cdot 10^{11}$	magnetostriction const.	λ_{100}		$7.0 \cdot 10^{-6}$

simulations. Magnetic hysteresis loops present the behavior of a magnetic material treated with a cycling, externally applied

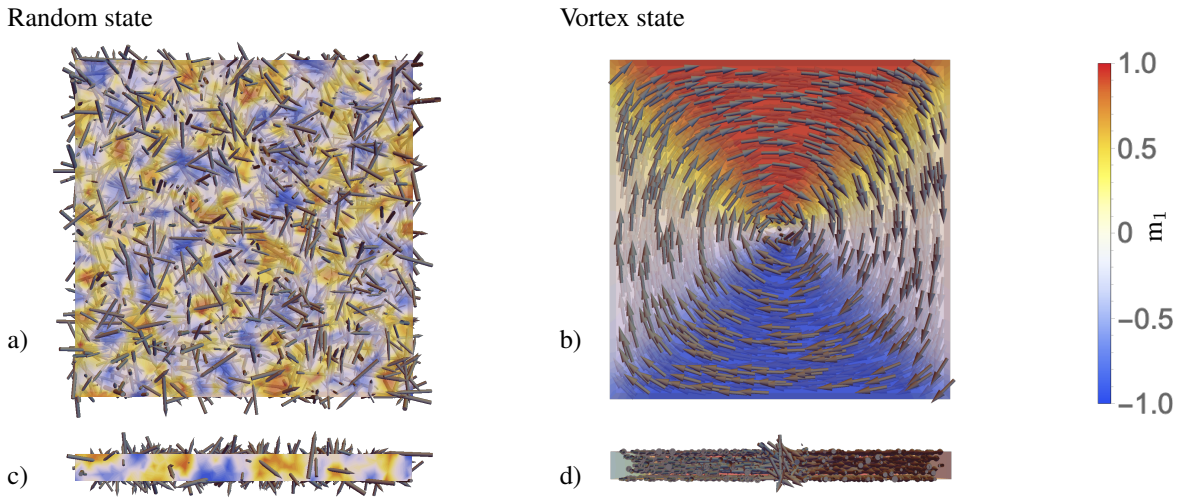

Fig. 1: A squared plate of Permalloy is initialized with an energetically high random magnetization state depicted in a) and c). The simulated relaxed or self-equilibrium state of the plate shows a vortex formation presented in b) and d).

magnetic field, revealing its distinct properties like the coercivity H_{c} or its remanence M_{r}. The influence of modified boundary conditions on the material behavior can also be well monitored by means of these hysteresis loops. Hence, the hysteresis of the nano structure is first calculated under homogeneous mechanical boundary conditions (free deformability of the structure). Subsequently, the nano structure is both compressed and stretched by applying a displacement of $u_{\mathrm{x}} = \pm 0.5\,\mathrm{nm}$ on $\partial\mathcal{B}_u$ within two independent simulations. The applied magnetic field has a field strength of $\mu_0\,\overline{H}_2 = 100\,\mathrm{mT}$ and follows the load path depicted in Fig. 2b. The resulting hysteresis loops of the three different boundary value problems are shown in Fig. 2a.

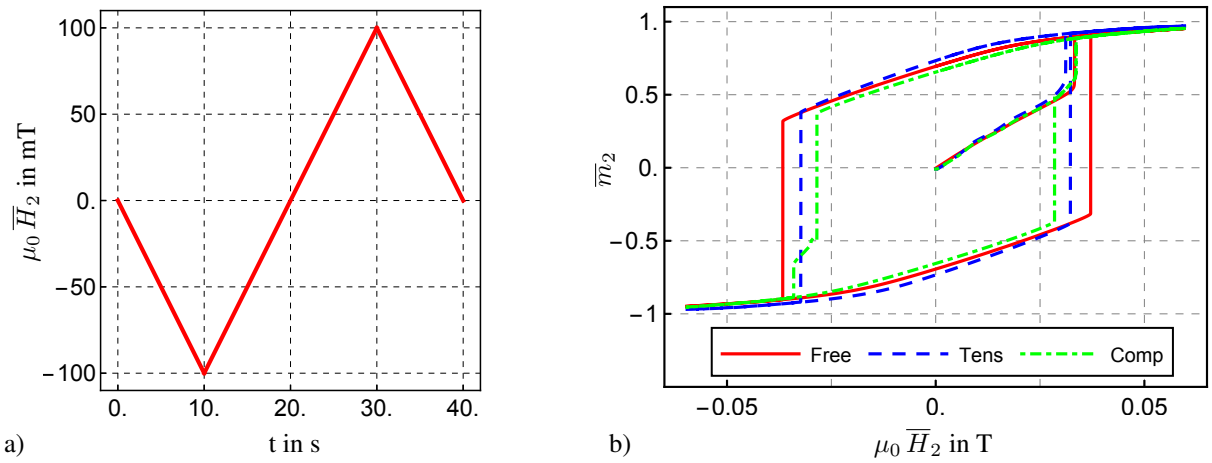

Fig. 2: a) Loading protocol following influence of an alternating externally applied magnetic field $\mu_0\,\overline{H}_2$ b) Influence of mechanical loading on the hysteresis.

The influence of the mechanical boundary conditions on the magnetic properties cannot be dismissed. Both tension and compression reduce the coercivity of the material. While the magnetization of the stretched nano structure switches entirely after a certain critical point, the compression causes a so-called kink to occur during the reversal. The influence of the mechanical boundary conditions on the results presented here will be considered more intensively in subsequent work. The presented examples illustrate how well the proposed model has worked so far. However, its performance still needs to be compared to the non-condensed perturbed Lagrange method. Therefore, the undeformed boundary value problem is recomputed, using the non-condensed perturbed Lagrange method. The condensed method delivers up to 10% faster simulations.

6 Conclusion

As an extension to the conventional Lagrange multiplier FE formulation of micromagnetics [22], a perturbed Lagrange multiplier approach is applied in this work. To improve computational efficiency, the introduced Lagrange multiplier was condensed using the Schur complement and the resulting local system matrix, reduced in dimension by one degree of freedom. The applicability of the presented model was sufficiently demonstrated by complex numerical examples. It was also shown that the computation time could be reduced by condensing the Lagrange multiplier. Future research will address the computational speed-up due to the condensation as well as the analysis of magneto-mechanically coupled hard and soft magnets.

Acknowledgements We gratefully acknowledge the financial support of the German Research Foundation (DFG) in the framework of the CRC/TRR 270, project A07 "Scale-bridging of magneto-mechanical mesostructures of additive manufactured and severe plastically deformed materials", project number 405553726. Open access funding enabled and organized by Projekt DEAL.

References

[1] O. Gutfleisch, M.A. Willard, E. Brück, C.H. Chen, S.G. Sankar and J. Ping Liu. Magnetic Materials and Devices for the 21st Century: Stronger, Lighter, and More Energy Efficient. *Advanced Materials*, **23**: 821–842, 2011.
[2] V. Franco and O. Gutfleisch. Magnetic Materials for Energy Applications. *JOM*, **64**: 750–751, 2012.
[3] H. Kronmüller. Theory of Nucleation Fields in Inhomogeneous Ferromagnets. *physica status solidi (b)*, **144**: 385–396, 1987.
[4] W.F. Brown. Micromagnetics (Wiley and Sons, New York, 1963).
[5] Homepage of CRC/TRR 270 HoMMage accessed on September 6th 2022. https://www.tu-darmstadt.de/sfb270/about_crc/index.en.jsp..
[6] L. Landau and E. Lifshitz.On the theory of the dispersion of magnetic permeability in ferromagnetic bodies. *Phys. Zeitschrift der Sowjetunion 8*, **2**: 153–169, 1935.
[7] T.L. Gilbert. A phenomenological theory of damping in ferromagnetic materials. *IEEE transact. on magnetics*, **40**: 3443–3449, 2004.
[8] M. Soderžnick, H. Sepehri-Amin, T.T. Sasaki, T. Ohkubo, Y. Takada, T. Sato, Y. Kaneko, A. Kato, T. Schrefl and K. Hono. Magnetization reversal of exchange-coupled and exchange-decoupled Nd-Fe-B magnets observed by magneto-optical Kerr effect microscopy. *Acta Materialia*, **135**: 68–76, 2017.
[9] T. Helbig, K. Loewe, S. Sawatzki, M. Yi, B. X. Xu and O. Gutfleisch. Experimental and computational analysis of magnetization reversal in (Nd,Dy)-Fe-B core shell sintered magnets. *Acta Materialia*, **127**: 498–504, 2017.
[10] J. Fischbacher, A. Kovacs, M. Gusenbauer, H. Oezelt, L. Exl, S. Bance and T. Schrefl. Micromagnetics of rare-earth efficient permanent magnets. *Journal of Physics D: Applied Physics*, **51**: 193002, 2018.
[11] A. Prohl, Computational Micromagnetism (Springer Fachmedien, Wiesbaden, 2001).
[12] A. Sridhar, M. A. Keip and C. Miehe. Homogenization in micro-magneto-mechanics. *Computational Mechanics*, **58**: 151–169, 2016.
[13] C.M.Landis. A continuum thermodynamics formulation for micro-magneto-mechanics with applications to ferromagnetic shape memory alloys. *Journal of the Mechanics and Physics of Solids*, **56**: 3059–3076, 2008.
[14] W. Dornisch, D. Schrade, B.-X. Xu, M.-A. Keip and R.Müller. Coupled phase field simulations of ferroelectric and ferromagnetic layers in multiferroic heterostructures. *Archive of Applied Mechanics*, **89**: 1031-1056, 2018.
[15] A. Vansteenkiste, J. Leliaert, M. Dvornik, M. Helsen, F. Garcia-Sanchez and B. Van Waeyenberge. The design and verification of MuMax3. *AIP Advances*, **4**: 107133, 2014.
[16] A. Inoue and F. Kong. Soft Magnetic Materials. *Encyclopedia of Smart Materials*, **5**:10-23, 2020.
[17] G.F Carey and J.T. Oden, Finite elements: a second course, Vol. II (Prentice-Hall, Engelwood Cliffs, 1982).
[18] P. Wriggers, Nonlinear finite element methods (Springer Science & Business Media, Berlin, 2008).
[19] D.P. Bertsekas, Constrained optimization and Lagrange multiplier methods (Academic press, 1982).
[20] J. Korelc and P. Wriggers, Automation of Finite Element Method (Springer, Berlin, 2016).
[21] H. Szambolics, L.D. Buda-Prejbeanu, J.C. Toussaint and O. Fruchart. A constrained finite element formulation for the Landau-Lifshitz-Gilbert equations. *Computational Material Science*, **44**: 253-258, 2008.
[22] D. Ohmer, M. Yi, O. Gutfleisch and B. X. Xu. Phase-field modelling of paramagnetic austenite–ferromagnetic martensite transformation coupled with mechanics and micromagnetics. *International Journal of Solids and Structures*, **238**: 111365, 2022.
[23] D. Sudsom, I.J. Junger, C. Döpke, T. Blachowicz, L. Hahn and A. Ehrmann. Micromagnetic simulation of vortex development in magnetic bi-material bow-tie structures. *Condensed Matter*, **5**: 5, 2020.
[24] C. Miehe and G.Ethiraj. A geometrically consistent incremental variational formulation for phase field models in micromagnetics. *Comput. Methods. Appl. Mech. Engrg.*, **245-246**: 331-347, 2012.
[25] T. Schrefl and J. Fidler. Modelling of exchange-spring permanent magnets. *JMMM*, **177-181**: 970-975, 1998.
[26] M. Kuchibhotla, A. Talapatra, A. Haldar and A.O. Adeyeye. Magnetization dynamics of single and trilayer permalloy nanodots. *Journal of Applied Physics*, **130**: 083906, 2021.

